

Multi-domain Polarization Switching in Hf_{0.5}Zr_{0.5}O₂-Dielectric Stack: The Role of Dielectric Thickness

Atanu K. Saha^{1,a)}, Mengwei Si¹, Peide D. Ye¹, and Sumeet K. Gupta¹

¹School of Electrical and Computer Engineering, Purdue University, West Lafayette, IN 47907, US

^{a)}Author to whom correspondence should be addressed: saha26@purdue.edu

ABSTRACT

We investigate the polarization switching mechanism in ferroelectric-dielectric (FE-DE) stacks and its dependence on the dielectric thickness (T_{DE}). We fabricate HZO-Al₂O₃ (FE-DE) stack and experimentally demonstrate a decrease in remnant polarization and an increase in coercive voltage of the FE-DE stack with an increase in T_{DE} . Using phase-field simulations, we show that an increase in T_{DE} results in a larger number of reverse domains in the FE layer to suppress the depolarization field, which leads to a decrease in remanent polarization and an increase in coercive voltage. Further, the applied voltage-driven polarization switching suggests domain-nucleation dominant characteristics for low T_{DE} , and domain-wall motion-induced behavior for higher T_{DE} . In addition, we show that the hysteretic charge-voltage characteristics of the FE layer in the FE-DE stack exhibit a negative slope region due to the multi-domain polarization switching in the FE layer. Based on our analysis, the trends in charge-voltage characteristics of the FE-DE stack with respect to different T_{DE} (which are out of the scope of single-domain models) can be described well with multi-domain polarization switching mechanisms.

Ferroelectric (FE) hafnium oxide, by virtue of its CMOS process compatibility^{1,2} and rich domain dynamics^{3,4}, has been identified as one of the most promising candidates for enabling future electronic devices. By integrating doped HfO₂ (as FE) in the gate stack of a transistor (FE-FET), non-volatile memory (NVM)⁵⁻⁶, neuron⁷ and synaptic^{8,9} functionalities have been demonstrated. Such diverse functionalities demand different characteristics of polarization (P) switching in the FE layer. For example, an abrupt P -switching is beneficial for neurons and binary NVMs, while a gradual P -switching is favorable for multi-bit memories and synapses. Therefore, it becomes essential to appropriately design FEFET for application-specific device behavior, for which gate stack optimization plays a key role.

In the FEFET gate stack, a dielectric (DE) layer exists between the FE and the semiconductor channel⁵⁻¹⁰, which can significantly impact the FEFET characteristics¹¹. According to the single-domain Landau-Khalatnikov (LK) model of FE, an increase in DE thickness (T_{DE}) should increase the depolarization field and reduce the coercive voltage (V_C) of the FE-DE stack^{12,13}. However, the FE-DE stack with Zr-doped HfO₂ (HZO) as the FE and Al₂O₃/HfO₂ as the DE have been demonstrated¹⁴⁻¹⁵ to exhibit an increasing coercive voltage (V_C) with the increase in T_{DE} . Therefore, it is important to bridge the gap between the theoretical understanding and experimental observations regarding the role of T_{DE} in FEFET and for that, a common approach is to analyze the FE-DE stack¹²⁻¹³. To that end, in this letter, we experimentally and theoretically analyze the P -switching in FE-DE stack with HZO as the FE and Al₂O₃ as the DE layer. Our results signify an increase in V_C , a decrease in remanent- P (P_R) and a decrease in P -switching slope with the increase in T_{DE} . By employing phase-field simulations, we show that such dependencies can be attributed to the multi-domain phenomena in FE¹⁶ which cannot be captured in the single-domain P -switching model. To further study the role of the dielectric, we analyze the dependence of V_C , P_R and the switching slope of the FE-DE stack on the dielectric permittivity through phase-field simulations.

For the fabrication of the FE-DE stacks, we start with the standard solvent cleaning of heavily p-doped Si substrates. Then, 30nm TiN layer is deposited by atomic layer deposition (ALD) at 250 °C, using [(CH₃)₂N]₄Ti and NH₃ as the Ti and N precursors, respectively. After this, an HZO film is deposited by ALD at 200 °C, using [(CH₃)₂N]₄Hf, [(CH₃)₂N]₄Zr, and H₂O as the Hf, Zr, and O precursors, respectively. HfO₂:ZrO₂ cycle ratio of 1:1 is used to form the 10nm Hf_{0.5}Zr_{0.5}O₂ film. Similarly, on top of HZO, an Al₂O₃ layer is deposited followed by a 30nm TiN layer deposition. After that, the samples are annealed at 500 °C in N₂ environment for 1 minute by rapid thermal annealing. Then, Ti/Au top electrodes are fabricated using photolithography, e-beam evaporation, and lift-off process (area=5024μm²). The average polarization (P_{avg}) versus applied voltage (V_{app}) measurement is carried out using a Radiant RT66C FE tester at room temperature at a very low frequency (50Hz). Considering the polarization switching time in HZO (<1μs)¹⁷, such low-frequency measurements can be considered as quasi-static. Fig. 1(a) shows the P_{avg} - V_{app} characteristics of FE-DE stack for 10nm HZO and 1/3/5nm Al₂O₃. Our results show a decrease in P_R (P_{avg} at $V_{app}=0V$), an increase in V_C (V_{app} at $P_{avg}=0$) and a decrease in P -switching slope with the increases in T_{DE} . To explain such dependencies, we now analyze the P -switching in the FE-DE stack based on multi-domain phase-field simulation.

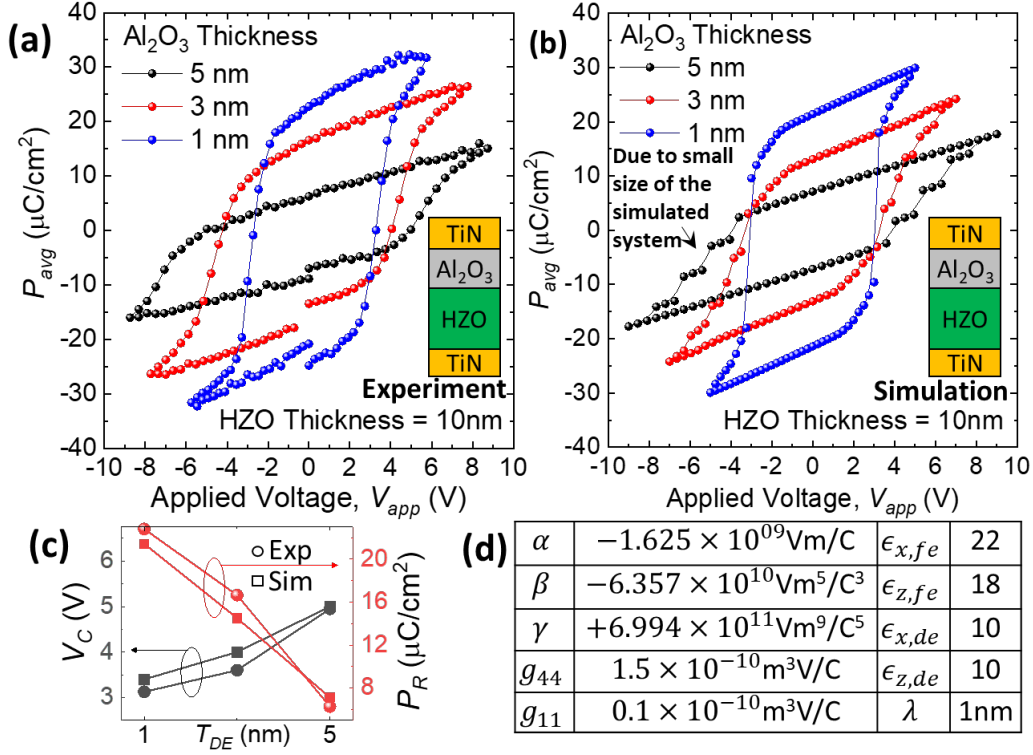


Figure 1: (a) Measured and (b) simulated P_{avg} - V_{app} characteristics of FE-DE stack for different T_{DE} . (c) average V_C (V_{app} at $P_{avg}=0$) and P_R (P_{avg} at $V_{app}=0$) for different T_{DE} . (d) Table showing the simulation parameters.

In our 2D phase-field simulation, we self-consistently solve the time-dependent Ginzburg-Landau (TDGL) equation (eqn. 1) and Poisson's equation (eqn. 2) as shown below^{18,19}.

$$-\frac{1}{\Gamma} \frac{\partial P}{\partial t} = \alpha P + \beta P^3 + \gamma P^5 - g_{11} \frac{d^2 P}{dz^2} - g_{44} \frac{d^2 P}{dx^2} + \frac{d\phi}{dz} \quad (1)$$

$$-\epsilon_0 \left[\frac{\partial}{\partial x} \left(\epsilon_x \frac{\partial \phi}{\partial x} \right) + \frac{\partial}{\partial z} \left(\epsilon_z \frac{\partial \phi}{\partial z} \right) \right] = -\frac{dP}{dz} \quad (2)$$

Here, α , β , and γ are Landau coefficients; $g_{11(44)}$ is the gradient coefficient; $\epsilon_{z(x)}$ is relative background permittivity; Γ is viscosity coefficient; ϕ is potential; P is the polarization of FE unit cell. We assume that the P -direction (c-axis of the orthorhombic HZO crystal) is parallel to the film thickness (z -axis)^{18,19}. Note that the dP/dz induces charges in the FE layer and thus enters in eqn. 2. At the FE-DE interface, $\lambda(dP/dz)-P=0$ is used for the surface energy contribution, where λ is the extrapolation length^{20,21}. All simulation parameters are given in Fig. 1(d). Due to the noncentrosymmetric crystal and lower elastic interactions in the out-of-plane direction compared to the in-plane direction in HZO²², we use $g_{11} < g_{44}$. Similarly, as the P -direction is along the z -axis, therefore, a lower number of atoms per unit cell take part in ϵ_z compared to ϵ_x and hence, $\epsilon_z < \epsilon_x$ (which is similar to other FE like PZT²³). We consider the length (l , along the x -direction) of the system to be 30nm which is analogous to the average grain size of HZO²⁴. To be consistent with the experimental measurements, the simulations are performed based on the quasi-static criteria (negligible dP/dt). Therefore, our simulation results are independent of the value of Γ . Further, we use a smaller FE region (equivalent to the size of a grain $\sim 30\text{nm}$) in simulation compared to the area of our experimental sample because of the scale-free nature of the FE HZO²². Thus, our simulations capture the trends with respect to the mean behavior of a single grain; however, for capturing the effects such as variation in coercive fields, a multi-grain simulation is needed which is out of the scope of this work. In the multi-domain scenario, P_{avg} is computed by integrating the displacement field at the metal-DE (or metal-FE) interface ($P_{avg} = \int \epsilon_0 \epsilon_{z,DE} E_{z,DE} dx / l = \int (P + \epsilon_0 \epsilon_{z,FE} E_{z,FE}) dx / l$). Here, the $E_{z,FE(DE)}$ is the out-of-plane (z) component of the electric field in the FE (DE) layer. The simulated P_{avg} - V_{app} characteristics of the FE-DE stack is shown in Fig. 1(b) illustrating a good agreement with the experiments (Fig. 1(c)). The mismatch in the P -switching region can be reduced by simulating multiple grains (discussed later).

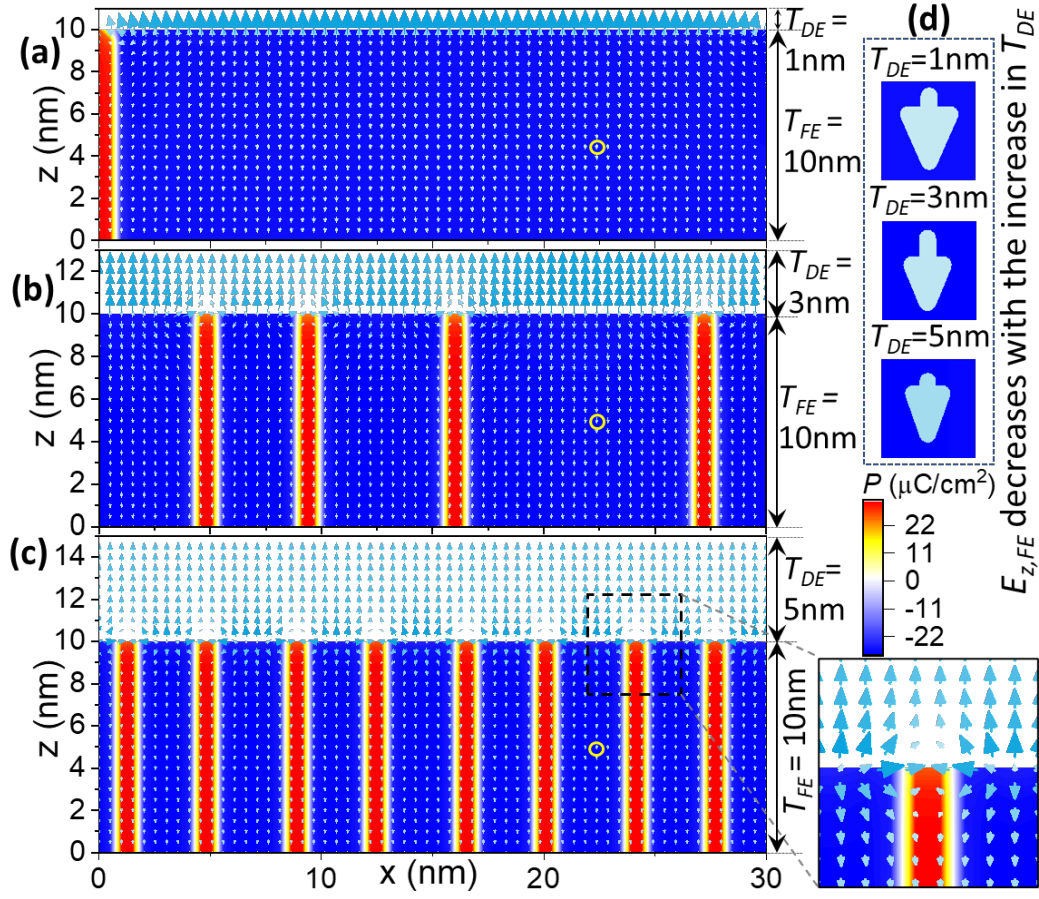


Figure 2: Simulated P (color map) and E -field (arrow) profile in FE-DE for $T_{DE} =$ (a) 1nm (b) 3nm, and (c) 5nm. The blue (red) regions signifying $-P$ ($+P$) domains. (d) $E_{z,FE}$ in FE at the yellow circle shown in (a-c).

To explain these characteristics, let us start with $V_{app}=0\text{V}$ and $P_R < 0$. In an FE-DE stack, the P -induced bound charges appear near the FE-DE interface leading to a non-zero $E_{z,DE}$ and $E_{z,FE}$. If P is homogeneous (e.g. in single-domain (SD) state), then $E_{z,FE}$ will be directed opposite to the P -direction yielding depolarization energy $f_{dep} (= -PE_{z,FE})$. At the same time, $E_{z,FE}$ will reduce the P magnitude ($|P|$) leading to an increase in the free energy (f_{free}). In order to suppress f_{dep} and f_{free} (to minimize the overall energy), FE breaks into multiple domains with opposite P -directions. In this multi-domain (MD) state, the P -induced bound charges at the FE-DE interface not only give rise to $E_{z,FE(DE)}$ (as before), but also form in-plane E -field ($E_{x,FE(DE)}$) called stray field^{18,25}. As a portion of the bound charge gets compensated by the stray-field, $E_{z,FE(DE)}$ is reduced in the MD state (compared to the SD state) leading to a reduction in f_{dep} and f_{free} . However, this suppression of f_{dep} and f_{free} occurs at the cost of (i) gradient energy, f_{grad} ($=g_{44}(dP/dx)^2$) due to the spatial variation of P in the domain-walls (DW) and (ii) electrostatic energy f_{elec} ($=\epsilon_0\epsilon_{x,FE}E_{x,FE}^2$) due to the stray fields. Hence, the formation of the MD state occurs as an interplay among competing energy components to obtain the minimum energy. With this understanding, let us now discuss the impact of T_{DE} on P_R .

In the FE-DE stack (at $V_{app}=0$ and $P_R < 0$), an increase in T_{DE} tends to increase $E_{z,FE}$ due to the higher voltage drop across DE and an equal and opposite voltage drop across the FE layer. This increase in $E_{z,FE}$ tends to increase f_{dep} and f_{free} . To counter this, a larger number of oppositely polarized domains ($+P$ in Fig. 2) appear that create more stray fields to suppress $E_{z,FE}$. The simulated P and E -field profiles in Fig. 2(a-c) validate the increase in the number of $+P$ domains (red domains) and suppression of $E_{z,FE}$ (Fig. 2(d)) with the increase in T_{DE} . The appearance of a larger number of $+P$ domains leads to a smaller size of $-P$ domains (blue) and hence, reduced $|P_R|$ with the increase in T_{DE} (Fig. 1(a-c)).

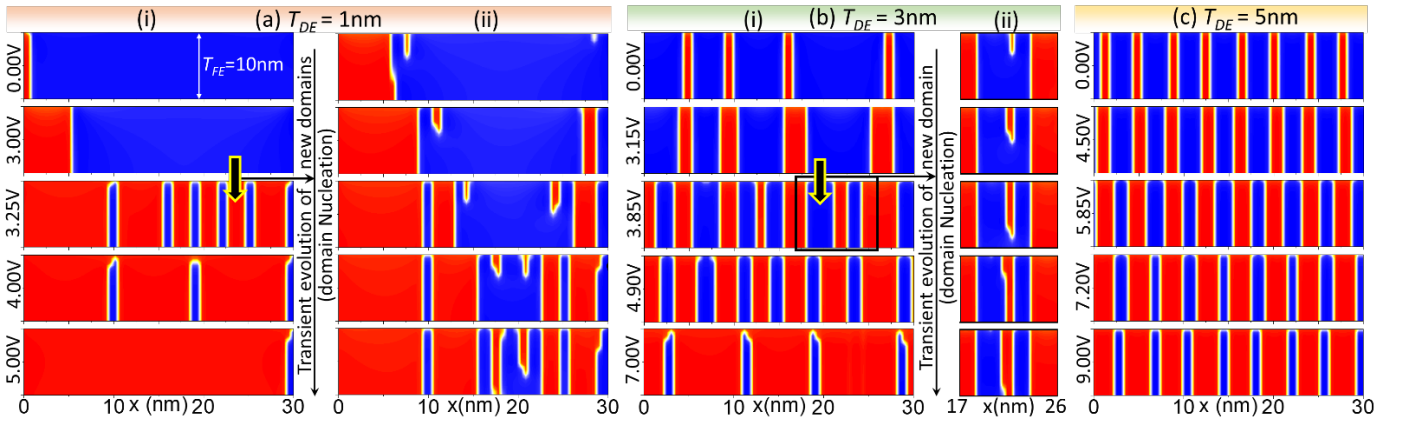


Figure 3: Simulated polarization profile in FE at a different applied voltage (V_{app}) in FE-DE stack for different T_{DE} = (a) 1nm, (b) 3nm and (c) 5nm showing domain nucleation and domain-wall motion based polarization switching. In all the cases, the FE thickness is 10nm.

Now, let us discuss V_{app} -induced P -switching. P -switching can take place if $f_{grad} + f_{dep} + f_{elec} + f_{free} > \max(f_{free})$. In the MD state, $E_{z,FE}$ is maximum away from DW near the FE-DE interface, which leads to maximum f_{dep} . In contrast, f_{grad} is maximum near the DW due to the largest variation in P . Now, with an increase in V_{app} , $E_{z,FE}$ increases leading to a change in P magnitude ($|P|$ increases in $+P$ domains and decreases in $-P$ domains). Thus, $f = f_{grad} + f_{dep} + f_{elec} + f_{free}$ increases¹⁶. If the increase in f is dominant near the DW, then P -switching occurs through DW motion. However, if the increase in f is dominant away from the DW, then P -switching occurs through the nucleation of new domains. P profiles at different V_{app} are shown in Fig. 3(a)-i for $T_{DE}=1$ nm. With the increase in V_{app} , P -switching starts through DW motion (at $V_{app}=1.5$ V) and at $V_{app}>3$ V several new domains nucleate causing a denser domain pattern. The transient nature of domain nucleation is shown in Fig. 3(a)-ii signifying their formation starting from the FE-DE interface. Once, the domain pattern becomes denser, a significant portion of $E_{z,FE}$ is suppressed by the stray fields at the expense of an increased f_{grad} . Hence, with further increase in V_{app} , P -switching takes place through DW motion leading to complete switching of several domains. Similarly, for $T_{DE}=3$ nm (Fig. 3(b)-i-ii), P -switching initiates through DW motion (at $V_{app}=1.85$ V) followed by domain nucleation (at $V_{app}>3.15$ V) and then DW motion. However, for $T_{DE}=5$ nm (Fig. 3(c)), the initial domain pattern is much denser, which suppresses $E_{z,FE}$ at the cost of f_{grad} . Hence, nucleation of new domains is not observed, and P -switching takes place only through DW motion (at $V_{app}>3.6$ V).

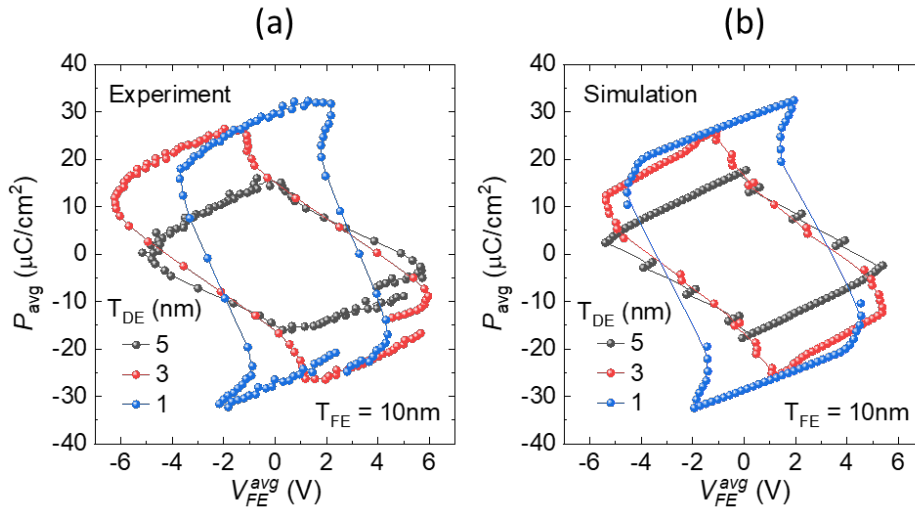


Figure 4: Extracted P_{avg} - V_{FE} characteristics of FE in the FE-DE stack from the (a) experimental and (b) simulated P_{avg} - V_{app} characteristics.

The extracted P_{avg} - V_{FE} characteristics from experimental and simulated P_{avg} - V_{app} characteristics are shown in Fig. 4 (a-b) signifying the negative dP_{avg}/dV_{FE} region. Such negative dP_{avg}/dV_{FE} exists during the P -switching in the FE layer via domain nucleation and/or DW motion. Recall that the local $E_{z,FE}$ in the FE layer is depolarizing i.e. opposite to the direction of P . Now, let

us consider the FE-DE stack is in the $P_R < 0$ state (average $E_{z,FE} > 0$). When V_{app} is increased and leads to MD P -switching, the P_{avg} increases either through the formation of new +P domains (nucleation) or through the size increase of +P domains (DW displacement). Both of these phenomena lead to a decrease in average $E_{z,FE}$ (i.e. the average $E_{z,FE}$ becomes less positive). As the increase in P_{avg} accompanies the decrease in average V_{FE} ($=T_{FE}E_{z,FE}$), thus the dP_{avg}/dV_{FE} becomes negative. A similar effective negative capacitance effect occurs for $P_R > 0$. It is important to note that the appearance of negative dP_{avg}/dV_{FE} is an electrostatic effect rather than a transient artifact. However, the actual slope of dP_{avg}/dV_{FE} can certainly be impacted by the frequency of the applied V_{app} due to the time-dependency of domain-nucleation and DW-motion.

The DW motion occurs via lattice-by-lattice propagation yielding a gradual increase in P_{avg} . However, the nucleation of a new domain involves simultaneous P -switching in several lattices leading to a sharper change in P_{avg} . Since, with an increase in T_{DE} , the dominant P -switching mechanism changes from nucleation to DW-motion-based, P -switching becomes more gradual - Fig. 1(a-b). Further, our simulations show a step-wise P -switching behavior for $T_{DE}=5\text{nm}$ (Fig. 1(b)), where each step jump signifies the DW displacement, and the flatter region corresponds to no DW displacement. The non-zero slope of the flat region is due to the response of P magnitudes and $\epsilon_{z,FE}$ to $E_{z,FE}$. In this flat region, with an increase in V_{app} , $E_{z,FE}$ first increases. If the increase in $E_{z,FE}$ is beyond a critical value so that $f > \max(f_{free})$, then the P -switching takes place via DW displacement. Recall that the P -switching leads to an increase in P_{avg} and a simultaneous reduction in $E_{z,FE}$. This yields a negative slope in the P_{avg} - V_{FE} characteristics ($dP_{avg}/dV_{FE} < 0$) and a step jump in the P_{avg} - V_{app} characteristics. Now, after each P -switching step, to induce further DW motion, V_{app} needs to be increased to increase $E_{z,FE}$ beyond a (new) critical value. Consequently, we observe a step-wise P -switching behavior in Fig. 1(b) and Fig 4(b). However, such step-jumps are absent in the measured characteristics because of the larger area (lots of grains) of the fabricated sample compared to our simulation (\sim one grain). Thus, even though the DW motion may be absent in some of the grains of the experimental sample, it may be present in other grains (due to the variation in grain size and/or crystallographic angle) leading to a continuous increase in P_{avg} . Hence, we expect that simulation of a larger system considering multiple grains may reduce this mismatch between the simulation and experimental results.

Let us now explain the effect of T_{DE} on V_C (defined as the V_{app} where $P_{avg} = 0$). For that, we consider the voltage drop across FE averaged along the length (referred as $V_{FE} = (\int \int E_{z,FE} dx dz) / l$). As an increase in T_{DE} suppresses $E_{z,FE}$ (discussed before), it leads to a decrease in V_{FE} at $V_{app} = 0\text{V}$. With the decrease in initial V_{FE} , a higher V_{app} is required to achieve a critical V_{FE} to trigger P -switching. Therefore, the DW motion initiates at $V_{app} = 1.5\text{V}$ for $T_{DE} = 1\text{nm}$ and at 1.85V for $T_{DE} = 3\text{nm}$. Similarly, the domain nucleation takes place at $V_{app} > 3\text{V}$ for $T_{DE} = 1\text{nm}$ and $V_{app} > 3.15\text{V}$ for $T_{DE} = 3\text{nm}$. Further, dP_{avg}/dV_{app} decreases with the decrease in T_{DE} (discussed before) leading to an increase in required V_{app} to achieve $P_{avg} = 0$. Due to the decrease in initial V_{FE} (at $V_{app} = 0\text{V}$) and lower dP_{avg}/dV_{app} , V_C of the FE-DE stack increases with an increase in T_{DE} . Note that the increase in V_C for larger T_{DE} cannot be captured by the SD mode, but can be described well considering the MD effects (as explained above).

So far we have discussed different attributes of P_{avg} - V_{app} characteristics of FE-DE stack with respect to different T_{DE} . This can also be regarded as the equivalent of different DE capacitances, $C_{DE} = \epsilon_0 \epsilon_{DE} / T_{DE}$. Now, one may argue that the P_{avg} - V_{app} characteristics can be also tuned by using a different DE material (ϵ_{DE}). While this is indeed possible (and can be an important design knob), the effect of ϵ_{DE} is not just changing C_{DE} , but involves some more physical processes that mandate further analysis. To decouple the effect of ϵ_{DE} on C_{DE} , we theoretically analyze the dependence of FE-DE characteristics on ϵ_{DE} in the supplementary sections by simultaneously and proportionally changing T_{DE} to keep the same C_{DE} . We show that the P_{avg} - V_{app} characteristics are not unique to C_{DE} , rather depends on the choice of ϵ_{DE} . Such dependency originates due to the electrostatic boundary condition of the in-plane electric field at the FE-DE interface. Considering different ϵ_{DE} (but same C_{DE}), our simulation results suggest that the V_C decreases and P_R increases with the decrease in ϵ_{DE} . We discuss such ϵ_{DE} dependency on the P -switching in FE-DE stack in the supplementary section.

In summary, we show that the FE layer forms a denser domain pattern with increasing T_{DE} by suppressing the depolarization field and leading to a higher hysteresis in the FE-DE stack. Simultaneously, the mechanism of P -switching can be modulated from nucleation to DW-motion dominant by increasing T_{DE} . In addition, we show that the DW energy and thus the coercive voltage and remanent P can further be modulated by ϵ_{DE} while keeping the same C_{DE} . Such T_{DE} and ϵ_{DE} dependency can serve as the potential knobs to deploy the application-driven optimization of the FEFET gate stack. For instance, FEFETs with low T_{DE} (high switching slope) can be used for the design of binary NVMs and neurons, while high T_{DE} can be utilized for multi-bit memories and synapse designs.

ACKNOWLEDGEMENT

This work was supported in part by Semiconductor Research Corporation (SRC) under contract no. 2020-LM-2959 and National Science Foundation (NSF) under grant no. 1814756 and grant no. 2008412.

DATA AVAILABILITY

The data that support the findings of this study are available from the corresponding author upon reasonable request.

REFERENCES

- [1] J. Müller, T. S. Böschke, S. Müller, E. Yurchuk, P. Polakowski, J. Paul, D. Martin, T. Schenk, K. Khullar, A. Kersch, W. Weinreich, S. Riedel, K. Seidel, A. Kumar, T. M. Arruda, S. V. Kalinin, T. Schlösser, R. Boschke, R. van Bentum, U. Schröder, and T. Mikolajick, *IEDM Tech. Dig.*, pp. 10.8.1–10.8.4, Dec. 2013. DOI: 10.1109/IEDM.2013.6724605
- [2] A. K. Saha, B. Grisafe, S. Datta, and S. K. Gupta, *Proc. IEEE VLSI Technol.*, pp. T226-T227, Jun. 2017. DOI: 10.23919/VLSIT.2019.8776533
- [3] K. Ni, B. Grisafe, W. Chakraborty, A. K. Saha, S. Dutta, M. Jerry, J. A. Smith, S. Gupta, and S. Datta, *IEDM Tech. Dig.*, pp. 16.1.1-16.1.4, Dec. 2018. DOI: 10.1109/IEDM.2018.8614527
- [4] A. K. Saha, K. Ni, S. Dutta, S. Datta, and S. Gupta, *Appl. Phys. Lett.*, vol. 114, no. 20, pp. 20903, May. 2019. DOI: 10.1063/1.5092707
- [5] K. Chatterjee, S. Kim, G. Karbasian, A. J. Tan, A. K. Yadav, A. I. Khan, C. Hu, and S. Salahuddin, *IEEE Electron Device Lett.*, vol. 38, no. 10, pp. 1379-1382, Oct. 2017. DOI: 10.1109/LED.2017.2748992
- [6] S. Dünkel, M. Trentzsch, R. Richter, P. Moll, C. Fuchs, O. Gehring, M. Majer, S. Wittek, B. Müller, T. Melde, H. Mulaosmanovic, Stefan Slesazeck, S. Müller, J. Ocker, M. Noack, D-A Löhr, P. Polakowski, J. Müller, T. Mikolajick, J. Höntschel, B. Rice, J. Pellerin, S. Beyer, *IEDM Tech. Dig.*, pp. 19.7.1-19.7.4, Dec. 2017. DOI: 10.1109/IEDM.2017.8268425
- [7] H. Mulaosmanovic, E. Chicca, M. Bertele, T. Mikolajick, and S. Slesazecka, *Nanoscale*, vol. 10, no. 46, pp. 21755-21763, Nov. 2018. DOI: 10.1039/C8NR07135G
- [8] H. Mulaosmanovic, J. Ocker, S. Müller, M. Noack, J. Müller, P. Polakowski, T. Mikolajick, and S. Slesazeck, *IEEE VLSI Technol.*, pp. T176-T177, Jun. 2017. DOI: 10.23919/VLSIT.2017.7998165
- [9] M. Jerry, P. Chen, J. Zhang, P. Sharma, K. Ni, S. Yu, and S. Datta, *IEDM Tech. Dig.*, pp. 6.2.1-6.2.4, Dec. 2017. DOI: 10.1109/IEDM.2017.8268338
- [10] P. Sharma, K. Tapily, A. K. Saha, J. Zhang, A. Shaughnessy, A. Aziz, G. L. Snider, S. Gupta, R. D. Clark, and S. Datta, *IEEE VLSI Technol.*, pp. T154-T155, Jun. 2017. DOI: 10.23919/VLSIT.2017.7998160
- [11] V. Gaddam, D. Das, and S. Jeon, *IEEE Trans. on Electron Devices*, vol. 67, no. 2, pp. 745-750, Feb. 2020. DOI: 10.1109/TED.2019.2961208
- [12] S. Salahuddin, and S. Datta, *Nano Lett.*, vol. 8, no. 2, pp. 405-410, Dec. 2007. DOI: 10.1021/nl071804g
- [13] A. K. Saha, S. Datta, and S. Gupta, *J. Appl. Phys.*, vol. 123, no. 10, pp. 105102, Mar. 2018. DOI: 10.1063/1.5016152
- [14] W. Xiao, C. Liu, Y. Peng, S. Zheng, Q. Feng, C. Zhang, J. Zhang, Y. Hao, M. Liao, and Y. Zhou, *IEEE Electron Device Lett.*, vol. 40, no. 5, pp. 714-717, Mar. 2019. DOI: 10.1109/LED.2019.2903641
- [15] M. Si, X. Lyu, and P. D. Ye, *ACS Appl. Electron. Mater.*, vol. 1, no. 5, pp. 745-751, May. 2019. DOI: 10.1021/acsaem.9b00092
- [16] A. M. Bratkovsky and A. P. Levanyuk, "Abrupt appearance of the domain pattern and fatigue of thin ferroelectric films," *AIP Conference Proceedings*, vol. 535, no. 1, pp. 218-228, Sep. 2000. DOI: 10.1063/1.1324458
- [17] M. Si, X. Lyu, P. R. Shrestha, X. Sun, H. Wang, K. P. Cheung, and P. D. Ye, *Appl. Phys. Lett.*, vol. 115, no. 7, pp. 072107, Aug. 2019. DOI: 10.1063/1.5098786
- [18] A. K. Saha, and S. K. Gupta, *Scientific Reports*, vol. 10, no. 1, pp. 10207, Jun. 2020. DOI: 10.1038/s41598-020-66313-1
- [19] H.W. Park, J. Roh, Y. B. Lee, and C. S. Hwang, *Adv. Mater.*, vol. 31, no. 32, pp. 1805266, Jun. 2019. DOI: 10.1002/adma.201805266
- [20] M. D. Glinchuk and E. A. Eliseev, *J. Appl. Phys.*, vol. 93, no. 2, pp. 1150, Dec. 2003. DOI: 10.1063/1.1529091
- [21] P. Chandra and P. B. Littlewood, *Physics of Ferroelectrics: A Modern Perspective*, *Topics Appl. Physics*, vol. 105, K. Rabe, C. H. Ahn, J.-M. Triscone, Eds., Berlin: Springer-Verlag, 2007, pp. 69-116. DOI: 10.1007/978-3-540-34591-6
- [22] H.-J. Lee, M. Lee, K. Lee, J. Jo, H. Yang, Y. Kim, S. C. Chae, U. Waghmare, J. H. Lee, *Science*, vol. 369, no. 6509, pp. 1343-1347, Sep. 2020. DOI: 10.1126/science.aba0067
- [23] A. I. Kurchak, E. A. Eliseev, S. V. Kalinin, M. V. Strikha, and A. N. Morozovska, *Phys. Rev. Applied*, vol. 8, no. 2, pp. 024027, Aug. 2017. DOI: 10.1103/PhysRevApplied.8.024027
- [24] H. J. Kim, M. H. Park, Y. J. Kim, Y. H. Lee, W. Jeon, T. Gwon, T. Moon, K. D. Kim, and C. S. Hwanga, *Appl. Phys. Lett.*, vol. 105, no. 19, pp. 192903, Nov. 2014. DOI: 10.1063/1.4902072
- [25] J. Íñiguez, P. Zubko, I. Luk'yanchuk, and A. Cano, *Nat. Rev. Mater.*, vol. 4, no. 4, pp. 243–256, Mar. 2019. DOI: 10.1038/s41578-019-0089-0

Supplementary Section

Multi-domain Polarization Switching in $\text{Hf}_{0.5}\text{Zr}_{0.5}\text{O}_2$ -Dielectric Stack: The Role of Dielectric Thickness

Atanu K. Saha, Mengwei Si, Peide D. Ye, and Sumeet K. Gupta

School of Electrical and Computer Engineering, Purdue University, West Lafayette, IN 47907, US

Effects of ϵ_{DE} in the P-switching characteristics in the FE-DE stack:

In this section, we discuss the effect of different DE permittivity (ϵ_{DE}) on the P switching characteristics of FE-DE stack while we keep the capacitance of the DE layer same (iso- $C_{DE} = \epsilon_0 \epsilon_{DE} / T_{DE}$). First, it is important to note that the electrostatic boundary conditions at the FE-DE interface need to satisfy not only the continuity of the out-of-plane displacement field ($D_{z,FE} = D_{z,DE}$) but also the equality of the in-plane electric-field ($E_{x,FE} = E_{x,DE}$). The in-plane interface E-field (E_x) between two opposite polarization domains (+P and -P) follows $|P| = \epsilon_0 \epsilon_x |E_x|$ and that implies an increase in E_x with the decrease in in-plane DE permittivity ($\epsilon_{x,DE}$). That, in turn, leads to an enhanced $E_{x,FE}$ and causes an increase in the in-plane electrostatic energy ($\epsilon_{x,FE} E_{x,FE}^2$) in the FE layer. Our simulation suggests that such an increase in in-plane electrostatic energy is partially compensated by reducing the P magnitude. However, this happens at the cost of an increase in the f_{free} . Overall, this leads to an increase in the local energy (f) near the DW for lower ϵ_{DE} (at iso- C_{DE}). This would imply that a smaller applied field (or V_{app}) will be required to initiate the P-switching in the FE-DE stack. Considering different ϵ_{DE} , our simulated P_{avg} - V_{app} characteristics are shown in Fig. S1 signifying that the DW motion initiates at a lower voltage with the decrease in ϵ_{DE} . Further, with the increase in coercive voltage of DW motion, the polarization switching via DW motion becomes more prominent for the lower ϵ_{DE} and same V_{app} . Consequently, the P_R increases with the decrease in ϵ_{DE} . It is important to note that the effect of ϵ_{DE} is more prominent in the case of lower C_{DE} (Fig. S1). This is because for lower C_{DE} (or higher T_{DE}) the P-switching mechanism is dominated by DW displacement and thus the change in the DW energy is more significant for lower C_{DE} . Note that such ϵ_{DE} dependency can be used as a potential knob to optimize the write voltage and retention of the FEFETs for NVM application.

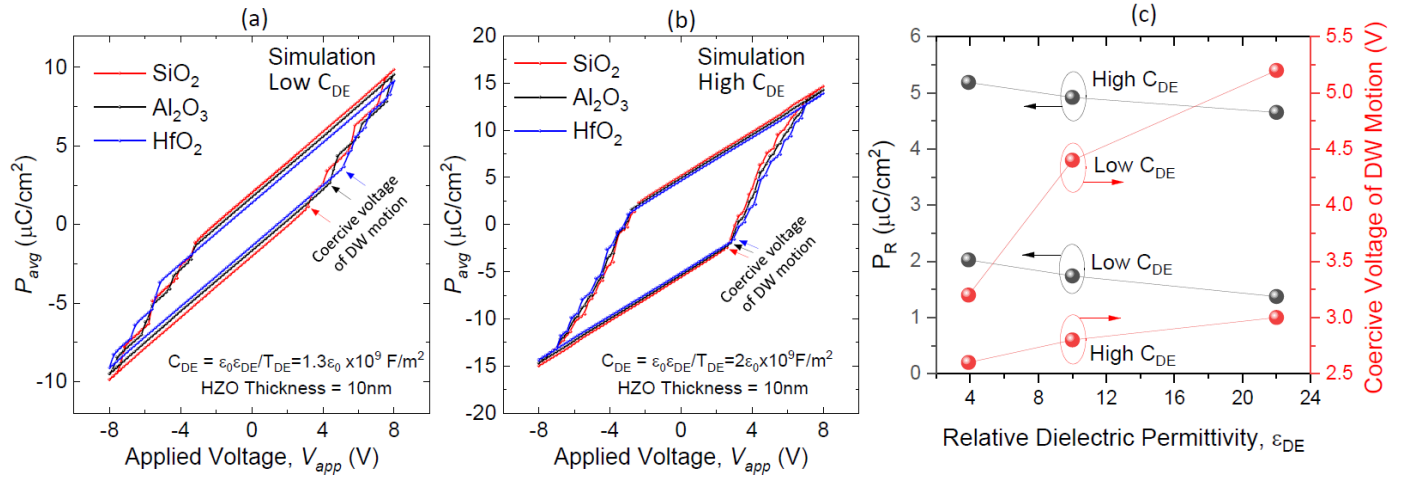


Figure S1: P_{avg} - V_{app} characteristics of FE-DE stack with different relative DE permittivity, ϵ_{DE} and iso- C_{DE} ($=\epsilon_0 \epsilon_{DE} / T_{DE}$) considering (a) $C_{DE} = 1.3 \epsilon_0 \times 10^9 \text{ F/m}^2$ (Low) and (b) $C_{DE} = 2 \epsilon_0 \times 10^9 \text{ F/m}^2$ (High). The coercive voltage of DW motion is shown as the arrow in (a-b). (c) The coercive voltage of DW motion and remanent P_{avg} (P_R) with respect to ϵ_{DE} for the low and high C_{DE} in Fig. S1 (a-b).